AIAA JOURNAL
Vol. 34, No. 10, October 1996

Pressure Field Around a Rectangular Supersonic Jet in Screech

Shojiro Kaji* and Noriyo Nishijima†
University of Tokyo, Tokyo 113, Japan

Supersonic jet screech generated by a rectangular nozzle with a pair of side walls added is studied both experimentally and numerically. A detailed observation of screech phenomena contributes to an understanding of the mechanism of sound generation. The numerical simulation shows that computational aeroacoustics is effective for strongly coupled flow acoustic problems such as screech. Flow visualization by an acoustically triggered pulse laser schlieren system clearly shows the dynamic motion of the third shock cell in the flapping mode. A traveling shock is found to exist in the third shock cell, and the sound is generated at the moment when the traveling shock coalesces into the end shock of the third shock cell. The instantaneous pressure distribution on the side wall shows that a pressure wave convectively propagates along the shear layer in the near field of the jet, while it propagates acoustically in the vertical direction away from the jet. Numerical simulation shows similar aspects of screech to those obtained in the experiment: the screech frequency, the flowfield, the fluctuating pressure distribution, etc. The calculated acoustic intensity shows that the acoustic energy is radiated at the end of the compression portion of each shock cell. The source of the first shock cell seems to supply the acoustic energy to its own shear layer to sustain the oscillation. It is also shown that the dimple spots observed in the isoamplitude contours of the screech sound pressure are a result of the interaction between discrete sources located at the end of each shock cell.

I. Introduction

POWELL[1] first described the mechanism of supersonic jet screech by using a feedback loop model, i.e., the development of instability waves in the shear layer, their interaction with the shock cell structure of the jet resulting in sound generation, and the excitation of instability waves at the nozzle lip by the sound propagating upstream. The component of this feedback loop was confirmed by shielding of sound propagation[2] or by enhancing sound effects by a reflector.[3] From flow visualization measurements,[4,5] the strongest sound source was found at the third or fourth shock cell.[5] The sound field around a circular jet was measured by Westley and Woolley,[6] and the source structure of a rectangular jet was investigated by Rice and Taghavi.[7] The acoustic far field[8] and the other characteristics of screech such as frequency, mode, directivity, and effects of nozzle shape have been studied by many investigators[7,9–13] (Ref. 13 gives a recent review of the subject).

Although Powell's feedback loop has been widely accepted, no satisfactory answers have been given to questions such as the following:

What does the interaction between instability waves and the shock cell structure actually mean?

How does the sound wave excite the instability wave?

Two different approaches can be used to answer these questions. One is the detailed observation and measurement of the flow and sound fields of the jet in screech. The other approach is to use numerical simulation of the supersonic jet in screech by solving Navier–Stokes equations. In the present study a rectangular supersonic jet, restricted by side walls, is used for the experiment, and the pressure field around the jet in flapping motion is measured on one of these walls. If the physical quantities do not change between side walls, the jet can be considered as purely two dimensional. However, because standing waves are possible between side walls, this situation may be different to some extent from rectangular free jets treated by former investigators.[2,5,7,8,12] For example, in the same experimental setup Suda et al.[14] found the symmetrical mode, which has never been observed in the free rectangular jet except for the case of impingement jets.[10] Numerical simulations are also carried out for a two-dimensional plane jet. The flowfield and the sound field are solved using the Navier–Stokes equations. Both experimental and numerical results show good agreement in many features of screech and also give some indication on the sound generation mechanism.

II. Experiment

A. Experimental Setup

The jet nozzle used for the experiment is the same as described in Ref. 14. The rectangular nozzle exit is 7 mm high and 72 mm wide. The nozzle walls are made of flat plates with the exit lip thickness of 14 mm, and the throat height is set to be 6 mm. Thus the perfectly expanded exit Mach number is about 1.8. In the case of visualization, glass side walls 290 mm high and about 300 mm long are set parallel to the jet at a distance of 72 mm apart.

In the case of pressure measurement, one of the side walls is changed as shown in Fig. 1. The wall is 390 mm high and 345 mm long downstream from the nozzle exit ($x = 0$). The part of the wall from $x = 9$ to 135 mm can be slid 160 mm in the vertical direction, on which the rotational wall of radius 60 mm is flush mounted within a limit of 0.05 mm. This rotational wall has a pressure transducer embedded at the radius of 54 mm. The pressure sensing hole is 0.5 mm in diameter and 1 mm long. A piezoelectric type pressure transducer is placed behind the sensing hole with 0.2-mm gap giving the Helmholtz resonance frequency higher than 10 kHz. The pressure transducer has sensitivity of 100 mV/10^5 Pa.

This traverse mechanism enables the measurement of unsteady pressure on the side wall in the region from $x = 18$ to 126 mm and from $y = -81$ to 29 mm in the coordinate system in Fig. 1 (the origin is the center of the jet at the nozzle exit). The x-wise

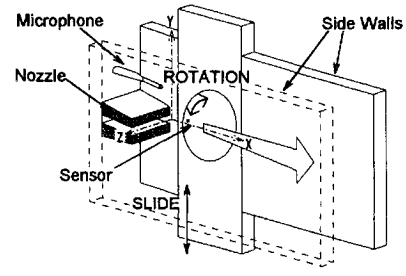

Fig. 1 Experimental apparatus and traverse mechanism.

Presented as Paper 95-020 at the CEAS/AIAA 1st Joint Aeroacoustics Conference, Munich, Germany, June 12–15, 1995; received Aug. 11, 1995; revision received May 29, 1996; accepted for publication June 3, 1996.

*Professor, Department of Aeronautics and Astronautics, 7-3-1 Hongo, Bunkyo-ku. Member AIAA.

†Graduate Student, Department of Aeronautics and Astronautics, Graduate School of Engineering, 7-3-1 Hongo, Bunkyo-ku; currently Research Engineer, Mechanical Engineering Research Laboratory, Hitachi Ltd., Tsuchiura, Ibaraki 300, Japan.

traverse is made every 3 mm, and the y-wise traverse is made every 2 mm from -30 to 30 mm and every 5 mm from -80 to -30 mm. The total of 1148 pressure data are obtained. A fixed microphone is placed above the nozzle exit at $x = 33$ mm and $y = 159$ mm to measure the screech sound, which is used as the reference signal. The phase of the pressure transducer output is counted relative to this reference signal. To do this we first determine the time interval between the start of data input and the time of zero voltage crossing (from negative to positive) for the microphone signal. Then the time scale of the pressure transducer output is shifted artificially by this time interval, and signal enhancement is made. Therefore, all pressure data can be referenced to a fixed time coordinate with the correct amplitude and phase. These pressure data can be used to obtain the instantaneous pressure contour on the side wall and to show the timewise variation of the pressure contour.

B. Flow Visualization

The flowfield around the jet and the sound field are measured by the acoustically triggered pulse laser schlieren system described in Ref. 14. As noted in the Introduction, the glass side walls introduced for visualization may change the flow condition so that it is different from that of a free jet. The results for the flapping mode indicate that the circular wave fronts are propagating as if they were emitted at the third shock cell (Fig. 2a). The detailed observation of the shock cell structure reveals that although the first and the second shock cells oscillate slightly, the third shock cell flaps dynamically with a traveling shock in it (Fig. 2b). This is confirmed by a video animation composed of 14 photos of different phases and is depicted in Fig. 3. First, the traveling shock A–B rotates around the point B and sweeps downstream (Figs. 3a and 3b). At the end of the half cycle, the edge of the traveling shock A reaches the downstream end of the cell, and this shock coalesces into the end shock of the third cell (Figs. 3c and 3d). Then, by this time a new traveling shock A′–B′ has been established, and the remaining half cycle proceeds in the similar manner. At this stage the traveling shock A′–B′ rotates around the point A′, sweeps downstream (Figs. 3d and 3e), and finally coalesces again into the end shock of the third cell (Figs. 3f and 3a). It is observed that a sound wave is emitted at the moment when the traveling shock coalesces into the end shock of the third cell. Recently, the oscillation of the shock in the circular jet has been measured, where splitting and merging of shock(s) are also recognized.[15]

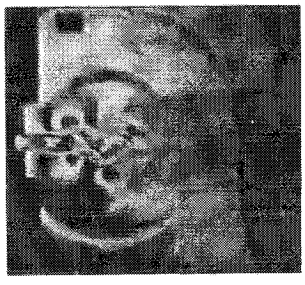

a) Sound field

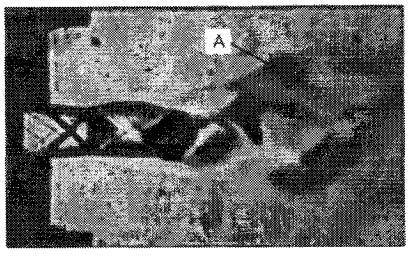

b) Flowfield, A = sound wave emission

Fig. 2 Flow visualization.

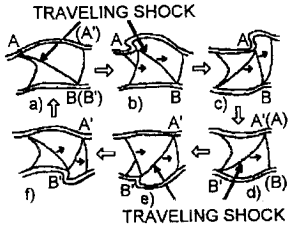

Fig. 3 Dynamic motion of traveling shock in third shock cell.

C. Spanwise Uniformity

To increase two-d.. ıensionality, side walls are added in this experiment. If physical quantities do not vary in the spanwise direction, purely two-dimensional conditions are satisfied. However, there is also a possibility for standing waves to be generated within the walls. In reality, it is difficult to get perfect uniformity in the spanwise direction. The spanwise variation of the screech pressure amplitude and phase is measured by the unsteady total pressure probe for the fundamental frequency and the first harmonic. This probe is essentially a stagnation-pressure-sensing pitot pipe of outer diameter 1.5 mm and inner depth 3.5 mm, which has a piezoelectric type pressure transducer inside aligned along the pipe axis. The resonance frequency of the pipe is higher than 14 kHz. The probe is directed to the jet nozzle, and the spanwise traverse is made at $x = 70$ mm and $y = -30$ mm.

Figure 4 shows the results. The nozzle pressure ratio (NPR) is 4.5. We see that a fairly uniform distribution is obtained for the fundamental component in this case. But when the NPR is changed from 4.5 to 4.75, the uniformity is destroyed considerably, and in the case of NPR = 5.0, the fundamental component shows an almost complete standing wave pattern as shown in Fig. 5. In addition, if we have any unbalance in the height of both side walls, no uniform distribution is obtained.

Figure 6 shows the x-wise distribution of the screech component when the more uniform spanwise distribution is obtained. We see that the screech pressure repeats peak and trough variation, reaching a maximum around $x = 70 \sim 80$ mm, and then decays downstream. The phase monotonically decreases from $x = 40$ mm downstream.

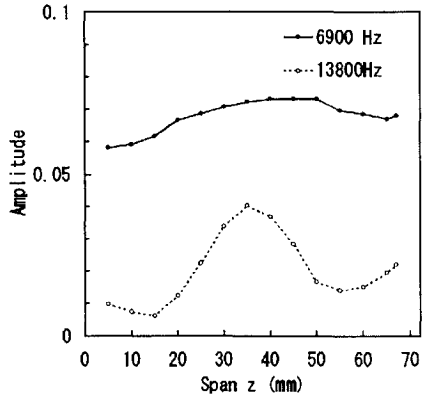

a) Amplitude

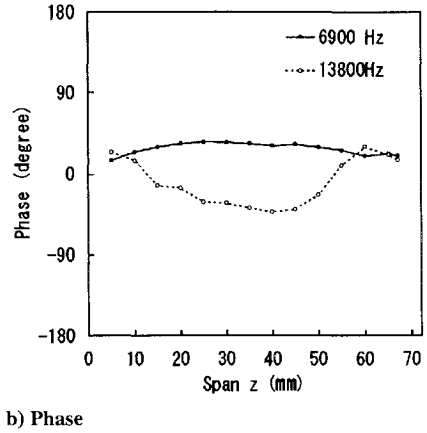

b) Phase

Fig. 4 Spanwise distribution of screech sound pressure, fundamental and first harmonic components: NPR = 4.5, $x = 70$ mm, and $y = -30$ mm.

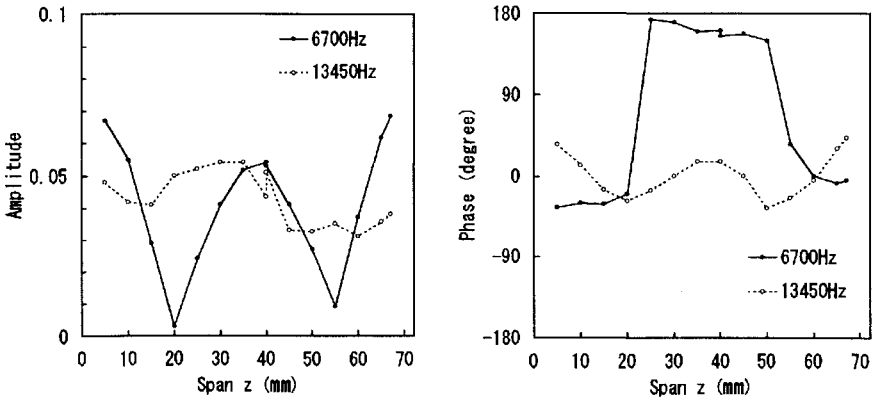

a) Amplitude b) Phase

Fig. 5 Spanwise distribution of screech sound pressure, fundamental and first harmonic components: NPR = 5.0, x = 70 mm, and y = −30 mm.

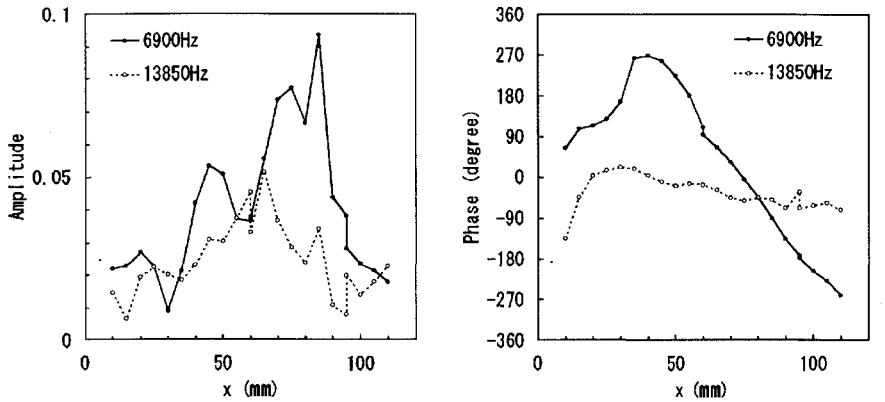

a) Amplitude b) Phase

Fig. 6 Streamwise distribution of screech sound pressure, fundamental and first harmonic components: NPR = 4.5, y = −30 mm, and z = 36 mm.

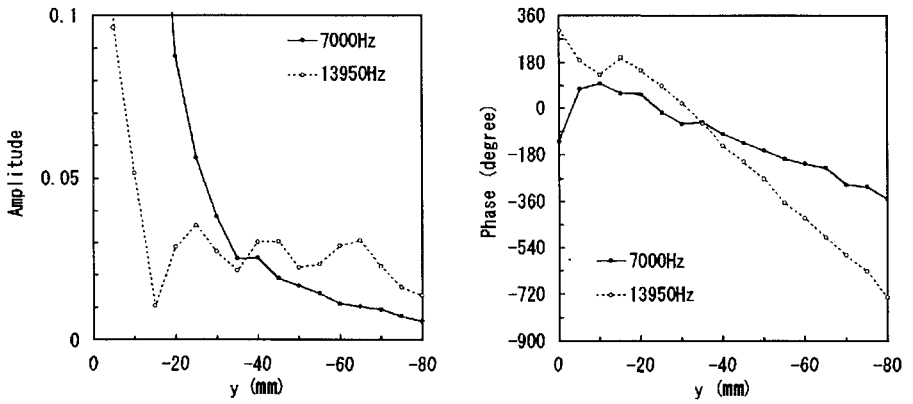

a) Amplitude b) Phase

Fig. 7 Vertical distribution of screech sound pressure, fundamental and first harmonic components: NPR = 4.5, x = 45 mm, and z = 36 mm.

The phase velocity measured from this delay is about 280 m/s. Figure 7 shows the distribution in the vertical direction. In the vertical direction the screech pressure amplitude decays monotonically away from the jet, and also the phase decreases steadily. The phase velocity in this direction is about 390 m/s.

D. Instantaneous Pressure Field

The unsteady pressure is measured on the side wall at the NPR of 4.5, where a fairly uniform spanwise mode is obtained. The following discussion is made assuming the flowfield and the sound field are both two dimensional. At this NPR the screech frequency is about 6950 Hz; therefore, the period is 144 μs and the acoustic wavelength in the free field is 49 mm. The shock cell length at this condition is about 19 mm. The pressure measurement is made in the region $x = 20$ to 101 mm and $y = -80$ to 30 mm, which covers fully the flapping jet from the second to the fifth (if present) shock cell.

Figures 8a and 8b show the instantaneous pressure distribution at $t = 0$ and 70 μs, respectively. We see that high- and low-pressure regions are located in a staggered fashion near the jet in the flapping mode and that they move downstream. After 70 μs (about a half period), the high- and low-pressure regions are entirely exchanged with each other.

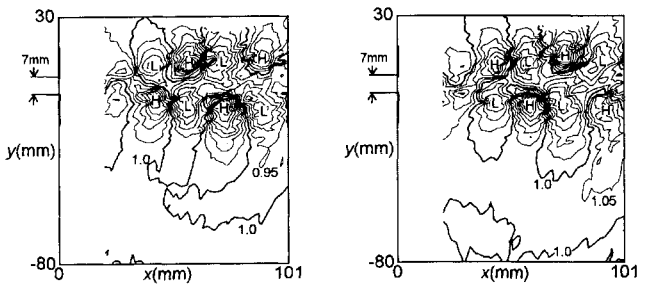

a) $t = 0$ μs b) $t = 70$ μs

Fig. 8 Instantaneous pressure distribution on side wall (contour spacing of 5000 Pa).

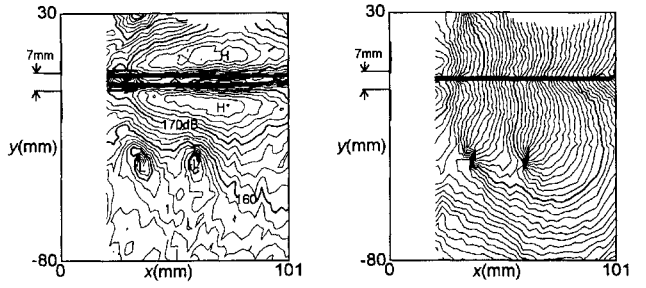

a) Isoamplitude contours (contour spacing of 2 dB) **b) Isophase contours (contour spacing of 20 deg)**

Fig. 9 Screech sound pressure distribution on side wall: NPR = 4.5 and 6933 Hz.

In the far field away from the jet, the high- and low-pressure regions spread outward alternately making circular wave fronts. Figures 9a and 9b show the isoamplitude and isophase contours, respectively, of the pressure measured on the side wall. The pressure level is high near the jet in the region where the jet experiences a violent flapping motion. Inside the jet the pressure level is relatively low (150–160 dB). Away from the jet the pressure level decreases gradually outward. There are dimple spots of low-pressure level in the region where the pressure field changes from near field to far field, i.e., almost one wavelength away from the jet. In the isophase contours, the bold line indicates the phase angle of 0 deg and other lines are drawn every 20 deg. We see that the upper and lower regions of the jet have opposite phase. Because waves proceed normal to the isophase line in the field without flow, we see that the pressure pattern moves almost parallel to the jet in the region near the jet. As the pressure propagates away from the jet, the direction of propagation changes from parallel to vertical to the jet. This means that the convective pressure field changes to the radiative pressure field. We see that there are singularity-like regions where all phase lines coalesce. These regions coincide with the low-pressure spots in Fig. 9a. We can recognize that the pressure wave propagates as if it turns around the singular spot.

III. Numerical Simulation

A. Method of Calculation

In the numerical simulation a two-dimensional planer jet is examined. The governing equation is the two-dimensional Navier–Stokes equation, which is written in conservation form as[16]

$$\frac{\partial Q}{\partial t} + \frac{\partial E}{\partial x} + \frac{\partial F}{\partial y} = \frac{\partial E_v}{\partial x} + \frac{\partial F_v}{\partial y} \tag{1}$$

where Q denotes the set of conservative variables, E and F are inviscid flux vector components, and E_v and F_v are viscous terms. Equation (1) is solved under curvilinear coordinate transformation, $\xi = \xi(x, y)$ and $\eta = \eta(x, y)$.

In this calculation laminar viscosity evaluated by Sutherland's formula is considered. No turbulence modeling is introduced. The explicit symmetric total variation diminishing scheme proposed by Yee et al.[16] is used. This code is second-order accurate in both time and space, but it shows good features in capturing shock waves.

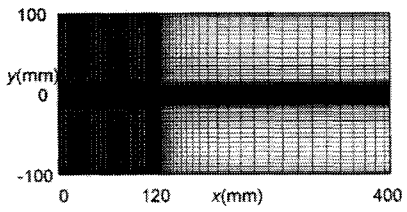

Fig. 10 Computational grid in physical domain.

Since this simulation treats an acoustic problem, we should avoid unnecessary reflection of physical quantities at computational boundaries. For this purpose, at boundaries except for the nozzle exit and nozzle lips, we adopt Thompson's nonreflecting type boundary condition.[17] His approach is based on the one-dimensional characteristic analysis. At the boundaries, inviscid flux components associated with normal directions are put in characteristic form and split into separate wave propagations. Outward propagating waves are calculated from the variables inside the computational domain, and as for the incoming waves, their amplitudes are kept constant. Tangential flux components at the boundaries are calculated in the same way as in the interior points. At the corners, ξ and η directions are, respectively, normal to the boundary; therefore, both flux terms are put in characteristic form. Because Thompson's scheme can be applied directly into nonlinear hyperbolic equations, this is favorable to the present study where the mean flow is unknown and strong interaction between flow and acoustic fields exists. However, Hixon et al.[18] recently pointed out that the performance of Thompson's scheme might only be acceptable when the flow is nearly one dimensional and perpendicular to the boundary.

The calculated flow conditions are as follows. The nozzle height is 7 mm, and the nozzle lip thickness is 13.5 mm. The nozzle exit Mach number is 1.5 at the NPR of 5. To stabilize the calculation a very slow coflow, Mach number 0.15 is added outside of the jet nozzle. We did not determine whether this Mach number could be reduced. At the nozzle lip an adiabatic wall boundary condition is applied, and at the nozzle exit, a uniform flow is assumed keeping all physical quantities constant.

The calculation region is 200 mm in the vertical direction, i.e., about 30 times of the nozzle height, and 400 mm in the flow direction, as shown in Fig. 10. The grid size is 211×141, out of which 181 points of x-wise meshes are gathered at equal intervals near the nozzle exit region between $x = 0$ and 120 mm, and 81 points of the y-wise meshes are allotted between $y = -10$ and 10 mm. Even when the fine mesh region in the x direction is extended from 120 to 240 mm, almost the same results are obtained in the region from $x = 0$ to 120 mm.

Initially the jet starts to issue from the nozzle exit and proceeds symmetrically to the outlet boundary. Then, this plume begins an asymmetrical motion and finally establishes a periodic flapping oscillation. It takes 5.125 ms and 30,000 iterations to establish the periodic motion, and the periodicity does not change up to 200,000 iterations, the maximum tried.

B. General Results

Figures 11a and 11b show, respectively, the instantaneous contour of the pressure and vorticity in the region near the nozzle exit between $x = 0$ and 120 mm. We see that the shock cell structure appears inside the jet and the discrete vortices start to roll up at around the third shock cell.

Figures 12a and 12b compare the spectrum of the pressure fluctuation. This spectrum is obtained by the fast Fourier transform analysis of the time history of the pressure at $x = 89$ mm and $y = 3.5$ mm for Fig. 12a. In this calculation the screech frequency is 5800 Hz. Besides higher harmonics, there appear subharmonics. The subharmonic component is very small near the nozzle exit region but increases along the jet flow. It is presumed, therefore, that the subharmonics are probably a result of nonlinear interactions (vortex pairing). However, we must be careful because the

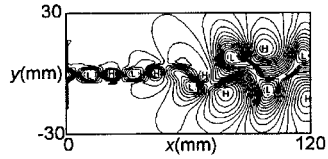

a) Pressure distribution

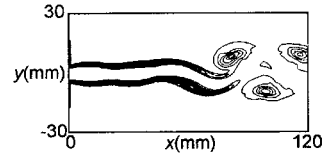

b) Vorticity distribution

Fig. 11 Calculated flowfield at $t = 8.206$ ms: NPR = 5.0.

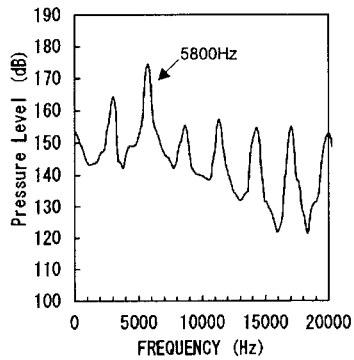

a) Calculation: NPR = 5.0, x = 89 mm, and y = 3.5 mm (fundamental screech frequency 5800 Hz)

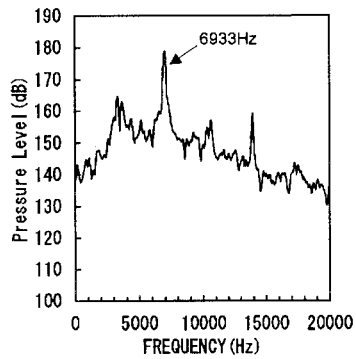

b) Experiment: NPR = 4.5, x = 62 mm, and $y = -10$ mm (fundamental screech frequency 6933 Hz)

Fig. 12 Comparison of frequency spectra for fluctuating pressure.

growth process of shear layers is sensitive to numerical conditions. For example, if we reduce the number of x-wise meshes in the fine mesh region (x = 0–120 mm) from 181 to 121, subharmonics disappear. Subharmonics are also observed in Fig. 12b measured at $x = 62$ mm and $y = -10$ mm in the experiment. But the variation of subharmonics in the flow direction does not necessarily show the increasing trend as found in the computational results, and further, at different locations the subharmonics sometimes vanish. Therefore, the appearance of subharmonics seems to be a phenomenon quite subtle and transitional.

Figure 13 shows the variation of screech frequency, predicted by the calculation, against the nozzle pressure ratio. Experimental results are also shown. Coincidence of both results is fairly good, showing the decreasing trend of the screech frequency against the NPR.

When we make an animation of the isopressure contours shown in Fig. 11a, we can actually recognize the pressure waves propagating outward and also upstream. But the physics can be best recognized

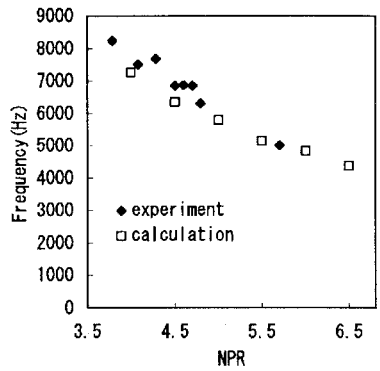

Fig. 13 Variation of screech frequency vs NPR.

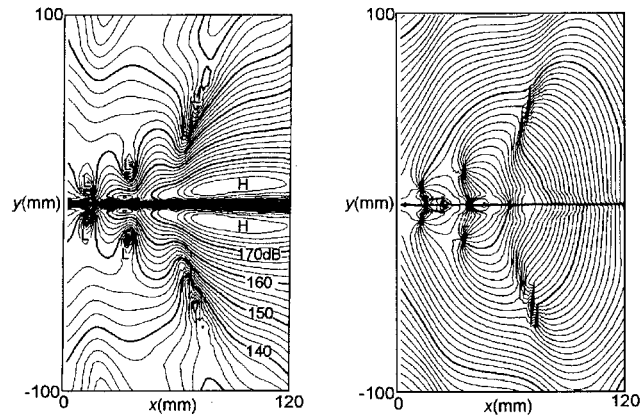

a) Isoamplitude contours (contour spacing of 2 dB)

b) Isophase contours (contour spacing of 20 deg)

Fig. 14 Calculated screech sound pressure distribution: NPR = 5.0 and 5800 Hz.

by the isoamplitude and isophase contours of the screech sound pressure, which correspond to Fig. 9.

Figure 14a shows the isoamplitude contours of the screech sound pressure and Fig. 14b the isophase contours. Again, we can recognize that the high-pressure region exists at the third or fourth shock cell near the jet and also a couple of low-pressure dimple spots exist away from the jet. From Fig. 14b, we see that these dimple spots correspond to the singularity-like regions of the isophase contours, where the pressure wave propagation changes from parallel to vertical to the jet. This tendency is surprisingly close to the experimental results of Fig. 9. Therefore, we can conclude that the numerical calculation can simulate the supersonic jet flowfield as well as the sound field of screech very well.

C. Acoustic Intensity

The acoustic intensity is the component of the time-averaged acoustic energy flux passing through the unit area. It gives a good measure of energy flow from source to the observer. In moving media the acoustic intensity can be expressed by the time-averaged total enthalpy flow[19]:

$$\bar{I} = \overline{[(p'/\rho_0) + \boldsymbol{u}' \cdot u_0](\rho_0 \boldsymbol{u}' + \rho' \boldsymbol{u}_0)} \qquad (2)$$

where ρ_0 and $\boldsymbol{u}_0$ are the mean density and velocity vectors and p', ρ', and $\boldsymbol{u}'$ are the fluctuating pressure, density, and velocity vectors, respectively. The acoustic intensity can be defined in the uniform flow, but not in a rotational or nonisentropic flow. However, we use here the acoustic intensity defined by the preceding equation.

Figure 15a shows the isomagnitude contours of the acoustic intensity vector. The highest intensity region is located on the shear layer of the second or the third shock cell. A single line interval indicates a 5-dB decrement. In the region inside the jet the acoustic intensity is low, and this is true especially in the upstream region of the potential core of the jet.

Figure 15b shows the direction of the acoustic intensity vector at each point. Comparing this figure with Fig. 14b, we can confirm that

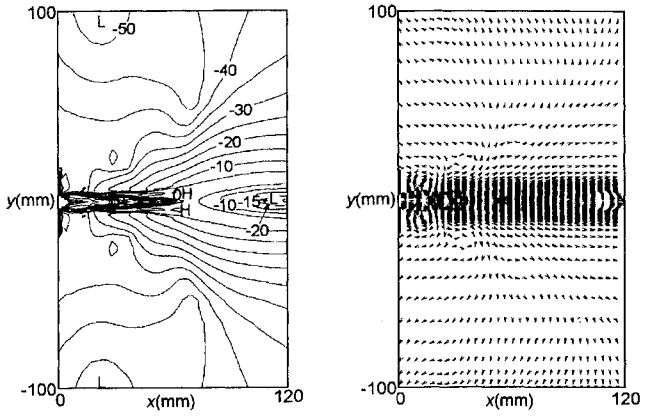

a) Isomagnitude contours (contour spacing of 5 dB) b) Direction

Fig. 15 Acoustic intensity vector: NPR = 5.0 and 5800 Hz.

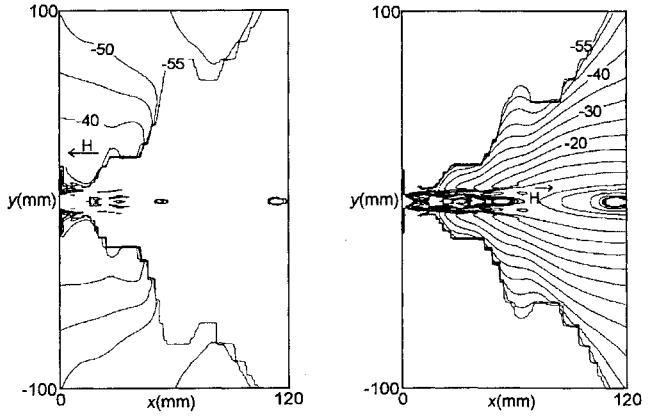

a) Negative x direction b) Positive x direction

Fig. 16 Isomagnitude contours of x-wise acoustic energy flow (contour spacing of 5 dB): NPR = 5.0 and 5800 Hz.

the acoustic intensity vector is directed almost normal to the isophase line. We see that at the end of each shock cell (compression region) the acoustic energy is radiated outward. This energy mainly flows downstream with the jet plume, but it is partly radiated in the vertical direction as well as in the upstream direction. The most important point is that the acoustic energy radiated at the end of the first shock cell comes back and enters the shear layer of the first shock cell.

Figures 16a and 16b show the contours of the x component of the energy flow. We see that the strongest intensity appears on the shear layer of the second or the third shock cell in Fig. 16b. This level is denoted by 0 dB. There is a zone along the line directed about 45 deg from the nozzle exit where the x-wise intensity becomes very weak. Across this zone the x-wise energy flow changes in direction from positive to negative. In Fig. 16a we see that a relatively high intensity region is located just outside of the jet, although the level is much lower than that in Fig. 16b.

Figures 17a and 17b show the contours of the y component of the energy flow. We find the strongest intensity is on the shear layer of the third shock cell. The positive y plot of Fig. 17b shows that energy spreads outward apart from the spots A and B, which are close to the singularity-like point in Fig. 14b. At these spots the reversal of energy flow occurs as shown in Fig. 17a. Looking at the region A where the y-wise energy is flowing in the negative y direction, we notice that the acoustic energy is supplied to the shear layer here since this region is in contact with the shear layer of the jet.

Thus we can conclude that although the shear layer (or rather vortex) at the third shock cell incorporates the strongest source region of screech, the source at the first shock cell seems to supply acoustic energy to the shear layer agitation. Further, this energy input occurs not just on the nozzle lip but on the entire region of the shear layer of

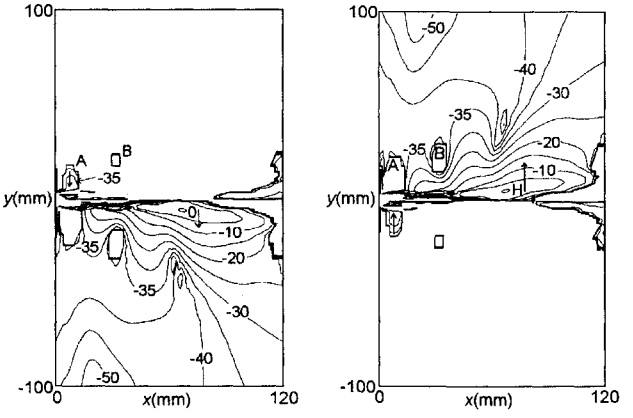

a) Negative y direction b) Positive y direction

Fig. 17 Isomagnitude contours of y-wise acoustic energy flow (contour spacing of 5 dB): A and B, spots of opposite energy flow; NPR, 5.0 and 5800 Hz.

the first shock cell. We must be careful, however, that the multiple sources at the end of each shock cell constitute synthetically the whole pattern of the energy flow.

IV. Discussion

In the experiment and the numerical simulation we find that two or three dimple spots of the isoamplitude contours of the screech sound pressure exist where the pressure phase behaves singularly. To show that these spots appear because of the interaction of multiple sources, we will perform a simple analytic calculation based on the following assumptions. This is similar to the approach taken by Powell.[1]

1) Simple acoustic sources are located at the averaged position of the shear layer (x_n, y_n) at the end of nth shock cell. Three sources $(n = 1, 2, 3)$ are considered. To express the antisymmetrical mode of jet oscillation, sources of opposite sign are placed at $(x_n, -y_n)$.

2) The amplitude of each source is proportional to $\exp[\alpha x_n]$, where x_n is the x coordinate of the position of the nth source and α is a constant representing the growth of the shear layer. This tendency is approximately shown in Fig. 6a.

3) Each source includes the phase factor $\exp[i\omega(t - x_n/C_v)]$, where ω is the circular frequency of the screech tone and C_v is the phase velocity in the downstream direction. Then, the pressure of the acoustic field can be expressed by

$$p(x, y, t) = \sum_{n=1}^{3} \exp\left[\alpha x_n + i\omega\left(t - \frac{x_n}{c_v}\right)\right] \times \left[H_0^{(2)}(kr_n) - H_0^{(2)}(kr_n')\right] \tag{3}$$

$$r_n^2 = (x - x_n)^2 + (y - y_n)^2$$

$$r_n'^2 = (x - x_n)^2 + (y + y_n)^2, \qquad k = \omega/a_0$$

where $H_0^{(2)}$ is the Hankel function of the second kind and a_0 is the velocity of sound.

Figures 18a and 18b show, respectively, the isoamplitude and isophase contours of the pressure based on the preceding equation. The value of α nondimensionalized by the source to source distance (i.e., the shock cell length) is 0.8. The nondimensional value of ω/C_v equals 1.2 times of $\pi/2$, which means C_v is equal to the jet velocity. We see that the low-pressure dimple spots appear and that the isophase contours show singular behavior there. Evidently these spots are generated by the interaction between sources. The radiation field is determined synthetically, and the second source shows forward radiation, whereas the third source has rearward directivity. Regarding the phase variation near the source line (the shear layer of the jet), the phase delays in the downstream direction are as assumed, but the density of phase lines is far from uniform when compared with the results obtained in the experiment (Fig. 9b). The

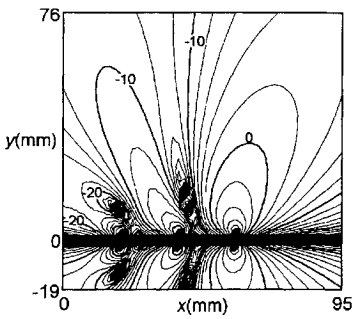

a) Isoamplitude contours (contour spacing of 2 dB)

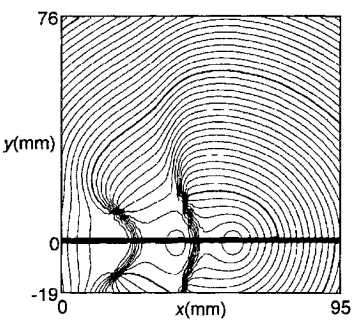

b) Isophase contours (contour spacing of 20 deg)

Fig. 18 Acoustic field generated by array of discrete sources. Source position: x = 19, 38, and 57 mm; $y = \pm 3.5$ mm; and 6950 Hz.

phase variation near the source line is close to that of the numerical simulation shown in Fig. 14b.

V. Conclusion

Supersonic jet screech phenomena are investigated both experimentally and numerically for a rectangular nozzle with side walls attached. Flow visualization and pressure field measurements confirm the screech characteristics known previously and reveal the existence of a traveling shock in the shock cell structure and also dimple spots in the pressure field. The numerical calculation has succeeded in predicting jet screech by solving the Navier–Stokes equations, and a good comparison with experimental results has been achieved. However, the numerical approach is far from quantitative, and the introduction of turbulence modeling, improvement of numerical accuracy in time and space, and improvement of radiation boundary conditions should be investigated. The important points obtained in this study are as follows.

1) The flow visualization indicates that there exists a traveling shock in the third shock cell, which undergoes dynamic motion interacting with the shear layer vortices. The pressure wave is radiated at the moment when the traveling shock coalesces into the end shock of the third shock cell.

2) The pressure measurement on the side wall confirms that the pressure pattern convectively propagates downstream near the jet while it propagates laterally away from the jet as the screech sound.

3) Two spots are found in the pressure distribution where the amplitude is low and the phase behaves singularly. The pressure wave propagation changes its direction around these points from parallel to vertical relative to the jet.

4) A numerical calculation based on the Navier–Stokes equation has been used to predict accurately various aspects of screech. Agreement of the results with the experimental measurements is very good, including the appearance of the spots in the pressure distribution described in the preceding paragraph.

5) The acoustic intensity indicates that the sound is radiated at the end of the compression portion of each shock cell. The acoustic energy flows downstream, but it is actually radiated outward and upstream. A part of energy radiated from the source at the end of the first shock cell goes into the shear layer region of the first shock cell.

6) The analysis based on the array of simple sources with the qualified amplitude and phase shows that the pressure distribution just described in point 3 is the result of the interaction between discrete sources.

Acknowledgments

The support for this study given by the Mitsubishi Foundation and also by the Grant-in-Aid for Developmental Scientific Research of the Ministry of Education are greatly acknowledged.

References

[1]Powell, A., "On the Mechanism of Choked Jet Noise," *Proceedings of the Physical Society, London*, Vol. 66, No. 408B, 1953, pp. 1039–1056.

[2]Hammitt, A. G., "The Oscillation and Noise of an Overpressure Sonic Jet," *Journal of the Aerospace Sciences*, Vol. 8, No. 9, 1961, pp. 673–680.

[3]Glass, D. R., "Effects of Acoustic Feedback on the Spread and Decay of Supersonic Jets," *AIAA Journal*, Vol. 6, No. 10, 1968, pp. 1890–1897.

[4]Ahuja, K. K, and Whiffen, M. C., "Tone Excited Jets, Part II: Flow Visualization," *Journal of Sound and Vibration*, Vol. 102, No. 1, 1985, pp. 63–69.

[5]Krothapalli, A., Hsia, Y., Baganoff, D., and Karamcheti, K., "The Role of Screech Tones in Mixing of Underexpanded Rectangular Jet," *Journal of Sound and Vibration*, Vol. 106, No. 1, 1986, pp. 119–143.

[6]Westley, R., and Woolley, J. H., "The Near Field Sound Pressures of a Choked Jet When Oscillating in the Spinning Mode," AIAA Paper 75-479, March 1975.

[7]Rice, E. J., and Taghavi, R., "Screech Noise Source Structure of a Supersonic Rectangular Jet," AIAA Paper 92-0503, Jan. 1992.

[8]Ponton, M. K., Manning, J. C., and Seiner, J. M., "Far-Field Acoustics of Supersonic Rectangular Nozzles with Various Throat Aspect Ratios," NASA TM-89002, Dec. 1986.

[9]Tam, C. K. W., Seiner, J. M., and Yu, J. C., "Proposed Relationship Between Broadband Shock Associated Noise and Screech Tones," *Journal of Sound and Vibration*, Vol. 110, No. 2, 1986, pp. 309–321.

[10]Norum, T. D., "Supersonic Rectangular Jet Impingement Noise Experiments," *AIAA Journal*, Vol. 29, No. 7, 1991, pp. 1051–1057.

[11]Morris, P. J., "Noise Radiation from Non-Circular Supersonic Jets," 14th Aeroacoustics Conf., DGLR/AIAA Paper 92-02-061, Aachen, Germany, May 1992.

[12]Raman, G., and Rice, E. J., "Instability Modes Excited by Natural Screech Tones in a Supersonic Rectangular Jet," *Physics of Fluids*, Vol. 6, No. 12, 1994, pp. 3999–4008.

[13]Tam, C. K. W., "Jet Noise Generated by Large-Scale Coherent Motion," *Aeroacoustics of Flight Vehicles: Theory and Practice*, NASA RP-1258, Aug. 1991, Chap. 6.

[14]Suda, H., Manning, T. A., and Kaji, S., "Transition of Oscillation Modes of Rectangular Supersonic Jet in Screech," AIAA Paper 93-4323, Oct. 1993.

[15]Panda, J., "Measurement of Shock Oscillation in Underexpanded Supersonic Jets," AIAA Paper 95-2145, June 1995.

[16]Yee, H. C., Klopfer, G. H., and Montagne, J. L., "High-Resolution Shock-Capturing Schemes for Inviscid and Viscous Hypersonic Flows," *Journal of Computational Physics*, Vol. 88, No. 1, 1990, pp. 31–61.

[17]Thompson, K. W., "Time Dependent Boundary Condition for Hyperbolic Systems," *Journal of Computational Physics*, Vol. 68, No. 1, 1987, pp. 1–24.

[18]Hixon, R., Shih, S.-H., and Mankbadi, R. R., "Evaluation of Boundary Conditions for Computational Aeroacoustics," *AIAA Journal*, Vol. 33, No. 11, 1995, pp. 2006–2012.

[19]Goldstein, M. E., *Aeroacoustics*, McGraw–Hill, New York, 1976, p. 41.